Icelandic Holuhraun plume: balloon borne measurement of aerosol size distribution

D. Vignelles1, T.J. Roberts1, E. Carboni2, E. Ilyinskaya3, P. Dagsson Waldhauserovà4, M. Pfeffer5, G. Berthet1, F. Jegou1, J.-B. Renard1, H. Olafsson6, B. Bergsson5, R. Yeo5, N. Fannar Reynisson5, R.G. Grainger2, B. Galle7, V.C. Jacobo7, S. Arellano7, T. Lurton1, B. Coute1 and Vincent Duverger1

1 LPC2E/CNRS / Université d'Orléans, 3A, Avenue de la Recherche Scientifique 45071 Orléans, France

2 COMET, Atmospheric, Oceanic and Planetary Physics, University of Oxford, Parks Road, Oxford, OX1 3PU, U.K.

3 British Geological Survey, Murchison House, West mains road, Edinburgh EH9 3LA, United Kingdom

4 Agricultural University of Iceland, Faculty of Environmental Sciences, Hvanneyri, Iceland

5 Icelandic Meteorological Office, Bústaðavegi 7-9, 150 Reykjavik, Iceland

6 University of Iceland, Icelandic Meteorological Office and Institute for Meteorological Research, Reykjavík, Iceland

7 Chalmers University of Technology, Department of Earth and Space Sciences, Hörsalsvägen 11, 412 96 Gothenburg, Sweden

Abstract.

In situ balloon borne flight measurements of the aerosols emitted by the Icelandic volcano Holuhraun plume have been realized on January 22nd 2015 at 21UTC. We present several data sets that we recorded during the balloon flight which intercepted the plume at 8km distance downwind from the crater, which represents a "young" plume age of approximately 15 minutes. We show in particular the aerosol size distribution measured by a novel miniature optical particle counter called LOAC (Light Optical Aerosol Counter) which determines both the number and size distribution of particles, alongside a meteorological payload. Compared with both local and distant independent SO_2 measurements, we discuss calculated aerosols flux emitted by Icelandic volcano.

The balloon passed through a plume located between 2 and 3.1 km in altitude above sea level. Two plume layers were observed, a non-condensed lower layer and a condensed upper layer. The lower layer of 400m thick was characterized by a modus of fine particles centered on 0.2µm in diameter and a second modus centered on 2.3µm in diameter and a total particle concentration

around 100 particles per cubic centimeter. The upper layer of 800m thick was a cloud-like signature with droplets centered on 20 µm in diameter and a fine modus, the measured total particle concentration was 10 times higher than the first layer. The plume top height was determined between 2.7 and 3.1 km, the plume height is in good agreement with an estimate made by analysis of IASI satellite remote sensing data.

This experimentation shows that under such difficult field campaign conditions (strong wind, low temperatures, only car batteries for power supply, night time and active volcano close to the launch site) it is possible to launch meteorological balloons with novel payloads to directly sample in-situ the near-source plume, determine the plume altitude, identify dynamical phases of the plume and document the size distribution of particles inside a plume which is only a quarter of an hour old.

1. Introduction

Volcanoes release gases and particles to the atmosphere through continuous degassing, or episodic eruption events, and depending on the injection altitude they can impact both tropospheric and stratospheric composition and climate. Ash-rich emissions such as the Icelandic Eyjafjallajökull eruption in 2010 can lead to widespread disruption of aviation (Spinetti et al., 2013). Ash-poor volcanic plumes can also strongly impact the environment and quality of life due to high concentrations of polluting gases and aerosol particles. Indeed, the recent 'Flood basalt' fissure eruption at Holuhraun (31 August 2014 – 27 February 2015, 1,6km^3 of eruptive lava, Gislason et al. 2015) was a major source of sulfur gases and aerosols and caused both local (Gislason et al. 2015) and European-wide (Schmidt et al. 2015) deteriorations to air quality.

Flood basalt eruptions are one of the most hazardous volcanic scenarios in Iceland and had enormous societal and economic consequences across the northern hemisphere. One of the best known examples is the Laki eruption (1783-84 CE) (Thordarson and Self, 2003) which caused the deaths of >20% of the Icelandic population by environmental pollution and famine (Thordarson and Self, 2003) and likely increased European levels of mortality through air pollution by sulfur-bearing gas and aerosol (Witham and Oppenheimer, 2004). Potential impacts of such an eruption on modern day Europe have been modelled by Schmidt et al. (2011) who found that PM2.5 aerosol pollution would double in concentration causing 142,000 (8-9%) additional cardiopulmonary fatalities in the year following eruption onset. A Laki-type eruption scenario has been recently included in the UK National Risk Register. However, there are still many uncertainties about the source terms of Icelandic flood basalt eruptions which are necessary for atmospheric models and health impact assessments. Holuhraun eruption was therefore a unique opportunity to study at first hand the near-source composition of a volcanic plume from an Icelandic flood basalt.

The capability of atmospheric models to predict volcanic plume impacts is limited by uncertainties in the near-source plume state. Most in-situ measurements of the elevated plume involve interception of more aged plumes that have already chemically or physically evolved. Small portable sensors airborne drone or balloon platforms offer a new possibility to characterize volcano plumes near to source. McGonigle et al. (2008) has demonstrated heli-type drone sensing of SO_2 and CO_2 to determine CO_2 fluxes at Volcano fumarole field. Recently, Shinohara (2013) deployed a suite of gas sensors on a drone to characterize the plume of Shinmoedake, Kirishima volcano, Japan during a hazardous eruptive phase that prevented ground-based sampling. Pieri et al. (2013) performed drone as well as balloon-based campaigns to measure gases and ash in the eruption plume of Turrialba volcano in Costa Rica. Measurements of volcanic aerosol (non-silicate particles, such as sulfate) are also needed to better constrain the plume sulfur chemistry and particle processes, which together with plume injection height are two key uncertainties in models used to predict the dispersion and

air-quality impacts from eruptions. Here we deployed a newly developed lightweight optical aerosol counter (LOAC) on a meteorological balloon through the Holuhraun eruption plume at source. Through measurements of size-resolved volcanic aerosol together with meteorological parameters we are able to provide key eruption source term information.

2. Methods

2.1 Balloon Instrumentation

The LOAC (Light Optical Aerosol Counter) is an optical particle counter sufficiently light-weight to be carried by a 1000gr meteorological balloon. The instrument contains a laser (650nm) and measures the intensity of light scattered at two angles, 12° and 60°, (Lurton et al., 2014; Renard et al., 2015) to discriminate the particle concentration over 19 size classes from 0.2 to 100µm in diameter. Sampling is made with a miniature pump (2 L/min) enclosed in the gondola, the air sampled is released after passing through the measurement cell. For the LOAC integration time of 10s, the counting uncertainty is derived from the Poisson counting statistics and defined as the relative standard deviation: 60% for aerosol concentration of 10^{-2} cm^{-3}, 20% for 10^{-1} cm^{-3} and 6% for concentrations higher than 1 cm^{-3}. A complete description of the instrument can be found in Renard et al. (2015). Differences in scattering between two distinct angles are also used to characterize the main nature of the aerosols (carbonaceous particles, sand, liquid droplets, salt), with reference to laboratory calibration samples, referred to as typology. As well as aerosol data, GPS coordinates, temperature and hygrometry are recorded in real time thanks to a telemetry system.

To aid interpretation, the balloon data are analyzed in conjunction with model outputs (trajectory, air quality plume dispersion and meteorological models) and remote sensing data (groung-based DOAS, and satellite IASI overpasses) as discussed in the Results.

3. Results

3.1 Holuhraun plume conditions

On January 22nd 2015, day of the balloon release, visible plumes were emitted from several different locations from the crater and lava field (figure1). The largest part of the emitted gas volume (about 90%) was released from the main vent named Baugur, where fresh magma was being erupted. The remaining gas emissions were sourced from the active lava flows traveling away from Baugur. These different plumes merged into one main plume that was advected northeastward. While it rose in altitude, the thermally buoyant plume visibly changed dynamical conditions, with the upper part of it turning into (an optically thick) cloud at several kilometers downwind from the source. The atmosphere was very clear within the boundary layer, and the lower troposphere was observed to be cloud-free except for the volcano plume cloud. Clouds were visible at much higher altitude (over 5.5 km as described in section 3.3.1). Figure 1 illustrates the Holuhraun plume as it was on January 22th at 14UTC. From the morning until the end of daylight, the plume exhibited visually very consistent behavior as described above. Atmospheric modelling (Iceland Met Office, CallPuff model, Barsotti et al. 2008.) predicted that the northeastward plume advection continued during the night, when our balloon-based measurements were performed (figure 2). Although this modelling output reflects the ground plume exposure, the constant vertical wind profile of the HARMONIE model in the Holuhraun zone (see discussion in section 3.3) justifies us to assume locally a similar plume dispersion from the ground up to 4 km altitude, as a guide to our balloon launching experiment.

3.2 Balloon flight

The meteorological balloon and measurement instrumentation were prepared during the evening of January 22nd, on site. The balloon was inflated during the night time, with a ground air temperature below 0° Celsius and relatively high wind speed of about 10m/s. The ground telemetry station was powered only by car batteries at this remote launch site. This situation was a combination of such difficult conditions for this kind of operation that making this balloon profile of the near-source plume represented a considerable challenge.

The balloon borne instruments were launched at 64°56'01"N & -16°40'39"E at 21 UTC on January 22nd 2015, 9 kilometers N-NE from the Holuhraun main eruptive crater (64°52'21"N & -16°49'42"E), and at around 700m above sea level. This launch site (directly under the plume) was chosen based on visual observations of plume advection made before night time, and output from the the HARMONIE model (figure 2). At this distance from the crater and given the dispersion of the plume, we were assured that a balloon launched from this location would cross the plume. Backward trajectories over the launching site confirm that the air mass movement was in the right direction, arriving from Holuhraun eruptive crater (figure 3). The backward trajectories are calculated with FLEXTRA 5.0 code which is a 3D kinetic trajectory calculation code (Stohl et al. 1999). Trajectories are initialized using global 3-hourly ECMWF reanalysis data with 1°x1° horizontal resolution for a period of 24h hours from 21 UTC on January 22nd and at every 200m above the balloon launching position up to 14 km. For clarity, Figure 3 presents only the backward trajectories initialized at 2400m and 4000m, corresponding to the height of the plume and the air mass above the plume respectively. It must be noted that all trajectories showed the same direction of advection indicating that the wind direction was similar between the ground to altitudes higher than the top of the plume (as determined by aerosol observations, see section 3.3). Based on the FLEXTRA backward trajectories, we were also able to determine the average age of the plume when the balloon crossed it, considering only a horizontal advection and constant velocity of the air mass between the two final hours of the trajectories. This calculation gives an air mass age between 10 and 15 minutes.

Physical parameters were recorded during the ascent and transmitted by telemetry. The meteorological parameters were recorded with a frequency of 1Hz whereas the particles concentration measured by the LOAC aerosol counter is given for each size class every 10 seconds and the typology relative to the optical properties of aerosols is provided every 60 seconds. The typology is a specific term relative to the index of optical particles refraction properties obtained by combining the intensities of light scattered at two specific angles (Renard et al., 2015). It can provide information on the nature of the particles, determined by reference to laboratory measurements (Renard et al., 2015). The typology gives several classes of optical properties discussed in section 3.4. Due to a technical problem with the data telemetry system, the concentration data was not recorded from the ground to around 1700m. Data were recorded from 1700m above the sea level (asl) to 8000m asl with a small number of data points lost during telemetry, mostly in the altitude range between 4.4 and 4.8 km asl.

3.3 Determination of zones

Figure 4 shows the vertical velocity of the balloon, the relative humidity (RH) and the total concentration of particles (TPC) between 0.2 and 100 µm in diameter as a function of altitude. On each plot we have determined 6 zones to discriminate several structures. These zones are represented by grey surfaces and numerated from the bottom on figure 4. These 6 distinct zones were determined based on correlations found between RH and aerosol profile. Figure 5 presents the observed aerosol size distribution as a function of altitude. For the size-dependent particle concentration, the number in each size class is represented by a color relative to the color scale on the left, the concentration is normalized by the range of size classes and is expressed as dn/dLog(d)

where n is the concentration and d the mean diameter of the class size. On the right panel, we show the optical typology detected by the LOAC for six groups of size classes. Each color represents the bulk nature of the aerosol shown by the color scale on the right of the graph. Most notable are two distinct zones of liquid droplets (around ~2.5-3 km altitude) and ice particles (around ~6-7 km altitude, zone 6) which correspond to distinct water/ice cloud layers. Further discussions of the aerosol size distribution and its typology across the identified zones are given in Section 4.

Zone 1 determined from 1.7 to 2.0km above sea level, presents a high and structured vertical balloon velocity profile, an increasing RH with altitude and a relatively low concentration of particles (around 5 particles per cm^{-3} over the 0.20µm to 100µm detection range). This zone is representative of the atmosphere near from the ground and under the plume.

Zone 2 from 2.0 to 2.3km above sea level, is characterized by a higher RH and higher particle concentration than the zone 1 (around 100 particles per cm^{-3}). The particle size distribution, discussed below, shows a second mode and the typology indicates a distinct mean nature of particles corresponding to absorbing particles. The zone 2 is the plume in a non-condensed phase.

Zone 3 is the plume in the condensed phase determined between 2.3 and 3.1 km above the sea level. The particle concentration is above 500 particles per cm^{-3}, and the typology indicates liquid droplets. This assumption is validated by the rapidly decreasing vertical velocity measured above 2.3 km which indicates a change in the air mass composition: above this altitude some liquid droplets condensed onto the balloon, increasing the mass of the balloon which caused the vertical velocity to decrease from 10 to 4 $m.s^{-1}$. This deduction is consistent with the hygrometry measurements which indicate a high RH above 2.3 km. The section 3.4 discusses the distribution in size measured in the zone 3 and shows clearly that the aerosols are composed by droplets. We determined the upper part of the zone 3 at 3.1 km even if the concentration of particles in 2.8 to 3.0 km band is close to the background level. We assume dynamical processes can locally modulate the aerosol concentration profile (plume layering). Here, the top of the plume is assumed to be between 2.8 and 3.1 km, which represents a very precise localization and is in good agreement with an estimate from satellite data as discussed further in section 3.3.2. In order to determine if zone 3 is a condensed plume or an atmospheric cloud above the eruptive location, we have used a non-hydrostatic convection-permitting model developed by Météo-France and ALADIN based on the AROME model from Météo-France (Seity et al, 2011, Brousseau et al. 2011) named HARMONIE. Firstly, outputs from the HARMONIE model for both 14UTC and 22UTC focused on the Holuhraun region confirms that the meteorological situation was very similar during the daytime when the photograph was taken (Figure 1) and nighttime when we launched the balloon, i.e. that there were no atmospheric clouds at this altitude. Figure 6 presents the temperature and the dew point for both day and night cases, showing very similar profiles in temperature, maximum dew point and wind direction at 14UTC and 22UTC. Secondly, the output from HARMONIE does not clearly indicate any low-level cloud. This model is not sensitive to the events such as Holuhraun eruption and therefore presents the meteorological conditions without the contribution of the volcanic plume. This result further confirms that the high aerosol and cloud droplets that we have visually observed at 14UTC and measured at 22UTC is actually the plume in a condensed phase visible on figure 1.

Zone 4 is the overlying air mass without the influence of the plume. A low total aerosol concentration was found in this zone, around 5 to 10 particles per cm^{-3} over the 0.20 µm to 100 µm detection range. This zone represents the background conditions and was found to be constant as a function of altitude even though the RH measurements still exhibit high values between 3.1 and 3.6 km which may be an instrument effect caused by persistence of humidity on the sensor. The

concentration and size distribution in this zone 4 is similar to the signature found in zone 1, thus the boundaries between zone 1-2 and 3-4 and determine the bottom and the top level of the plume.

Zone 5 and 6 are discussed here only briefly in order to show the complete profile of flight. Between 4.4 and 4.9km we lost the signal from the gondola. Zone 5 is assumed to be a background air mass influenced by the icy cloud determined by zone 6. The typology clearly identifies the particles to be icy cloud in zone 6 corresponding to the high altitude clouds visible on figure 1.

4. Discussion

4.1. Plume Height

Our balloon-based measurement of plume height (2 and 3.1km, with condensed phase layer between 2.3km and 3.1km) is a key constraint needed for models of the downwind plume dispersion. We compare our plume height observation to an independent estimate of the plume height as well as the SO_2 column analysis from IASI data on METOP Satellite. This novel technique to retrieve plume height from satellite data is described by Carboni et al. (2012) and has been applied to several volcanic eruptions in Carboni et al. (2015). Here we only report a summary of the algorithm. The optimal estimation technique of Rodgers (2000) is employed to estimate SO_2 plume, and the surface skin temperature using simultaneously all IASI measurements from 1000 to 1200 cm^{-1} and from 1300 and 1410 cm^{-1} (the v_1 and the v_3 SO_2 bands). The retrieval is effected by minimizing a cost function J defined as

$$J = (\mathbf{y} - \mathbf{F}(\mathbf{x}))\, \mathbf{S}_y^{-1}\, (\mathbf{y} - \mathbf{F}(\mathbf{x}))^{-1} + (\mathbf{x} - \mathbf{x_a})\, \mathbf{S}_a^{-1}\, (\mathbf{x} - \mathbf{x_a})^{-1}$$

Where **F(x)** is the forward model (i.e. the function which maps the state parameters to measurements), **x** is the vector of retrieved values, **y** the measurement vector, $\mathbf{S_y}$ is the measurement error covariance matrix, $\mathbf{x_a}$ is the a priori error covariance matrix. The forward model is based on RTTOV (Saunders et al. 1999) extended to include SO_2 explicitly, and uses ECMWF temperatures interpolated to the measurement time and location. Note that the SO_2 IASI retrieval is not affected by underlying cloud and rigorous error propagation, including the incorporation of forward model and forward model parameter error, is built into the system, providing quality control and error estimates on the retrieved state for every pixel. Figure 7 shows the contribution of three overpasses of METOP over Iceland on January 22nd at 18, 19 and 20 UTC (within hours of our balloon flight). Each measurement is represented by a symbol and a color. Symbols are relative to the hour where the satellite overpassed (a star for 18 UTC, a cross for 19 UTC, a diamond for 20 UTC). Colors represent the retrieved plume altitude. The altitude given by the Carboni algorithm of the closest measurement from the crater is 3.0 ± 1.1 km. This altitude is consistent with the altitude detected by the LOAC which determines the top height of plume in the 2.7-3.1 km range, although the two estimates are based on data collected 30 kilometers apart. Thus the LOAC balloon flight contributes to the in-situ validation of the recently developed Carboni et al. (2012, 2015) method for the plume altitude estimation by IASI satellite retrieval. Altitude estimation of volcanic plumes is critical both for modelling plume advection, chemical processing and atmospheric impacts, and can be a key uncertainty in the estimation of SO_2 burdens from satellite.

4.2. Particle size distribution in the plume

In this section we investigate the size-distribution in the different altitude zones in detail. Figure 8 presents the particle size distribution in zones 1 to 4. The left panel shows the size distribution in each zone averaged across the number of points that were recorded by telemetry during the ascent and presented in dn/dLog(d). Every 10 seconds the LOAC measures a distribution in size over 19 size

classes from 0.2 to 100 µm, these data are presented in the left panel with thin grey lines and the mean average shown with thick black line with diamonds. On the right, for each average size distribution we have calculated the volume distribution assuming spherical particles with diameter centered on the mean diameter of the size class. For each volume distribution we fitted log normal distribution modes described by equation (1), also shown in the right panel of Figure 8 table 1.

$$V(d) = \frac{V_0}{\sigma_N \sqrt{2\pi}} e^{\left(-\frac{1}{2}\left(\frac{\log(d)-\mu_v}{\sigma_N}\right)^2\right)} \quad (1)$$

Where $V(d)$ is the volume density distribution with shape parameters: σ_N and μ_v and the amplitude parameter V_0 were determined by least-squares fitting to the LOAC observations.

Firstly, we observe that the size and volume distributions for zones 1 and 4 (both identified as background air, outside of plume) are of similar proportions, with similar mean diameter and standard deviation. The difference in total number of particles between the zone 1 and 4, higher in smallest size for the zone 1 closer to the ground, is likely due to wind erosion and different aeolian processes. Holuhraun is located northward from the largest Icelandic Glacier Vatnajokull in the largest desert area of Iceland called Dyngjusandur (Arnalds, 2010; Baratoux et al., 2011; Dagsson-Waldhauserova et al., 2013, 2014). Dyngjusandur consists of sand dominated by glass grains from several volcanic eruptions of Askja, Bardabunga and Kverfjoll in the past (Baratoux et al., 2011; Oladottir et al., 2011), while a mixture of volcanic materials was likely added also during the Eyjafjallajokull 2010, Grinsvotn 2011 and Holuhraun 2014-2015 eurptions. Dyngjusandur dust is frequently suspended during storms (Dagsson-Waldhauserova et al., 2013). These dust events occurred, however, mostly during the summer-autumn period, whilst resuspension of snow may be a wind-driven surface source of particles in winter. We assume that this mono-modal background particle distribution is also a representative background for zones 2 and 3 where plume was present. Clear bimodal particle distributions are observed in these zones 2 and 3, which dominate over the background signature. The bimodal distribution consists of sub-micron and supra-micron modes in zone 2, attributed to non-condensed plume. In the condensed plume of zone 3 these modes have greater diameter.

More precisely, zone 2 presents a size distribution that is higher in number than the zone 1 for particles smaller than 1µm, with the first mode maximum below detection range (< 0.2 µm), and with a second mode around 2 µm (all parameters are summarized in Table 1). This observation is strikingly similar to ground-based observations of volcanic aerosols in the plume of quiescently degassing Mt Etna, made using a hand-held LOAC instrument at ~1 km downwind from the volcano summit (Roberts et al., 2015), a similarly bi-modal distribution was found, with similar sub-micron and supra-micron modes. Interestingly, our Holuhraun measurements made 8km from the source observe a greater proportion of particle volume in the smaller mode relative to the larger mode than for the Etna measurements made just ~1km from the source. This difference might reflect a greater extent of near-downwind plume processing during the 15 min (8km) plume transport but might also reflect differences in the nature of these two volcanic emission sources (which vary in both emissions, strength and composition). Further observations of a range of volcanic plumes under different conditions are needed to distinguish these two possible explanations.

The zone 3 condensed plume exhibits a first mode at somewhat greater diameter than in zone 2, and a second mode with diameter 19 µm. Such particle modes around 10 µm are characteristic of clouds (Warner 1969, Hammer et al. 2014). Typology clearly shows the existence of liquid droplets.

Water cloud droplet formation is expected given presence of submicron particles even in the background air as well as the plume that can act as cloud condensation nuclei also noting the Holuhraun eruption produced very little ash. The measured vertical concentration profile in the zone 3 might be affected by an instrumental effect called the shadowing effect that lead to underestimate the number of fine particles when larger particles are simultaneously detected (due to a scattering coincidence effect in the measurement cell see Renard et al. 2015, and Roberts et al., 2015 who identified this effect under strong volcanic plume conditions). In addition, a reduced number of small particles in the presence of larger particles might indicate the process of fine particles growing into larger particles leading to a transfer from the smallest size to larger. The phenomenon is significant between 2.4km and 2.7km where large particles in the first layer of condensed plume appear, see Figure 4, 5. This part of zone 3 is flanked by two peaks with fewer large particles and greater than 10 times the concentration of smaller particles than the inner region where a greater number of large particles are detected. It is also indicative of plume heterogeneity.

Above the plume in zone 4, the particle size distribution is relatively constant and close to the distribution in size measured in zone 1 (with typology shows high complex refractive index relative to absorbing particles), until the icy cloud becomes present between 5.5 and 7 km (zone 5). This occurs in a region of higher RH and is highlighted both by both the size-resolved aerosol number and the speciation index, Figure 5.

4.3. Optical particles index, the "Typology"

For zone 2, the speciation index relative to the optical properties of particles does not reveal a clear optical nature of particles. It gives optically absorbing signature, however we believe the observed particles to be most likely dominated by sulfate, based on particle measurements from non-explosive ash-poor volcanic emissions made elsewhere (e.g. Kroll et al., 2015). Volcano emissions are chemically reactive and the sulfate aerosol can be formed through high-temperature near-vent chemistry as well as low-temperature atmospheric oxidation of emitted SO_2 (e.g. Roberts et al., 2014). A possible complexity to determining speciation from particle scattering can be the presence of internally mixed aerosol, or particles of different kinds in the same sampling period. Volcanic aerosol can be a complex mixture, with sulfate typically as a major component but also containing e.g. metal salts. Roberts et al. (2015) determined that the LOAC measurements of aerosol in Etna grounding plume were fully consistent with having a predominantly aqueous sulfate composition (as determined from volume calculations with co-measured SO_2), but also observed an absorbing signature in the LOAC typology, proposed to be caused by additional contaminants within the sulfate aerosol which can have a disproportionate effect on the overall typology. However, no further conclusion on the precise Holuhraun particle composition can be made here. Nevertheless, the result is that the nature of the particles are distinct between zones 1 and 2. Certainly the plume did not contain substantial quantities of volcanic ash. This is confirmed by the quiescent nature of the degassing (in stark contrast to the explosive Icelandic Eyjafjallajökull eruption of 2010 see Spinetti et al. 2013) and in-field visual observations made during the eruption. The reddish-brown hue of the plume in Figure 1 is most likely attributed to an optical effect of back-scattered sunlight from the aerosols.

In zone 3 the typology gives an unambiguous droplets signature. Here the condensed phase is clearly established. This also confirms the hydroscopic nature of the volcanic particles. Condensed water on the volcanic particles both increases their size (section 3.3) and acts to dilute any absorbing component to the extent that the typology yields a droplets signature.

The typology is less well resolved over the altitude profile than the concentration but also indicates the same plume layering: in the 2.8-3.0 altitude range where a thin layer of non-condensed plume was found (section 3.3).

Typology is similar for the zone 4 and zone 5. Typology for zone 6 is also very well established as being distinct to the previous zones and indicates ice. The presence of icy clouds at high altitudes is thus clear.

4.4. Particle flux

Over the 1 km thick non-condensed part of the plume (zone 2) the LOAC instrument measured on average about 100 particles per cm^{-3} over the class size range 0.2 to 100µm in diameter. Using this particle concentration observation we attempt a calculation to coarsely estimate the particle emission from Holuhraun. This cannot be calculated directly from the aerosol and plume depth observations because the width of the plume is unconstrained. Neither was SO_2 co-measured during the LOAC balloon flight, therefore the calculation is only approximate. We calculate a ratio number of particles per kg of SO_2 by comparing the balloon-based aerosol observations to remote sensing SO_2 observations by DOAS scanning the plume 10 km from the crater and from IASI satellite, and combine with the total flux of SO_2 released in January 2015 to finally estimate the number of particles emitted on the whole period.

The NOVAC scanning DOAS (Galle et al. 2010) is positioned 10 km eastward from the Baugur vent (64°53'3.78"N; 16°40'31.70"O). The scanning NOVAC DOAS instrument uses scattered sunlight in the UV region to derive path-integrated concentrations (columns) of SO_2. The instrument's viewing direction is rotated along a conical surface from horizon to horizon. When this cone intersects a plume, the total number of molecules of SO_2 in a cross section of the plume can be determined, and the flux through the cross section was calculated with the NOVACProgram software using wind speeds and directions determined by the HARMONIE numerical prediction model and a plume height of 1387 m, which is the average triangulated plume height when two DOAS instruments detected the plume. Column SO_2 density of up to 800 DU (time average of 200 DU) was detected on the day of the flight (one Dobson unit (DU), is equivalent to 2.69×10^{16} molec.cm-2 SO_2 column). An average emission rate of 400 kg/s SO_2 for this day was calculated using wind parameters provided by the HARMONIE numerical prediction model. Assuming 200 DU SO_2, 100 particles per cm^{-3} and plume of 1km thick, a ratio of 1.75×10^{13} particles per kg of SO_2 is calculated. Combining with the 400 kg/s SO_2 flux yields a coarsely estimated flux of 6×10^{20} volcanic particles in the range of 0.2 and 100 µm emitted by Baugur vent during this day. The same estimation with IASI data at 2 DU SO_2 (figure 7) gives 10^{15} particles per kg of SO_2 and 6×10^{22} particles emitted during this day. Two magnitudes of difference on these estimations can be due to the difference in the field of view of the methods and the non-collocation of measurements. The IASI data is representative of a more aged plume 30 km away, that may be physically and chemically evolved. The DOAS SO_2 column may thus be more representative of the nearer source plume, however, our measurement in situ aerosol measurement in the non-condensed plume (zone 2) will also depend on whether the balloon flight sampled the more concentrated plume center or dilute plume edge. For comparison, Roberts et al. (2015) reports ~10^{15} particles of 0.20 – 100 µm size range per kg SO_2 at Mt Etna made by co-measured in-situ aerosol and SO_2.

The Holuhraun 2014-15 eruption emitted at least 3 times more SO_2 per day than the total of all anthropogenic SO_2 sources across 28 European countries in 2010 (European Environmental Agency (EEA), 2014). Fluxes of SO_2 have been reported of up to 120 kilotons per day (kt/d) in September 2014 (reducing to 20-60 kt/d between 6 and 22 September 2014), with an overall emission of 2.0 ± 0.6 Tg of SO_2 during the month of September and 11±5 Tg of SO_2 for the whole active period (Gíslason et al. 2015). We highlight that if our particle/SO_2 ratio, ~10^{13}–10^{15} particles (0.2-100µm

range) per kg SO_2 in the near-downwind plume estimated for 22 Jan 2015 is representative for the volcanic source for the whole eruption period this yields a flux of up to ~10^{22}-10^{24} particles per month from Holuhraun, but further aerosol formation will occur by atmospheric oxidation of SO_2 as the plume is dispersed and advected downwind, impacting both the free troposphere and ground-level air quality at both local and regional scales (Schmidt et al., 2015). The particle surface area also plays an important role in plume heterogeneous chemistry (Roberts et al., 2014), as well as climate impacts (Schmidt et al., 2012).

5. Conclusion

This study demonstrated that the newly developed light balloon borne aerosol counter LOAC is an effective method to detect and characterize a volcanic plume close to the crater. We have shown that with this method, we were able to determine with a great accuracy the height of the top and the bottom of the Holuhraun plume at a very specific location and time, and identify and characterize distinct layers in the plume as a result of different hygroscopic phases of the plume based on the observed aerosol size distribution.

Volcanic plumes are known to impact cloud formation and cloud properties through volcanic sulfate aerosol that act as cloud condensation nuclei , (Martucci et la. 2012, Spiridonov et al. 2013). However, for our observations the cloud rather likely formed due to the presence of hygroscopic volcanic particles and excess water vapor in the near-source plume, noting volcanic emissions commonly predominantly consist of H_2O with typically only <1 to 10 % sulfur compounds, typically mostly as SO_2, e.g. Oppenheimer et al. (2011). For this near-source emission into a cold atmosphere, the gaseous H_2O emission condenses onto the volcanic sulfate particles as the plume rises and cools to lower temperature (resulting in higher RH). Such cloud formation may facilitate processes (e.g. within cloud droplet SO_2 oxidation) that could alter the plume properties and downwind impacts. Clouds are commonly observed on top of volcano summits, but their formation can simply be due to orographic reasons, here the volcanic origins are evident.

We thereby demonstrate a new launch-on-command capacity for the combined volcano particle and plume height characterization during major volcano eruption events that can be applied near to source as shown in this study but also to the dispersed plume further downwind. Other flights including a LOAC passing through volcanic plumes are under investigation. Meteorological balloons with LOAC instrument payloads can be launched by non-specialist personnel and are low-cost compared to other methods such as by aircraft, and can be operated under a wider range of volcano hazard conditions. This method can potentially be used to sample the near-source volcano plume of a large eruption that is being injected into the stratosphere. Several LOAC balloon payloads are being kept ready for launch in Iceland and France as well as near volcanoes overseas (e.g. the island of la Reunion) in preparation for future major eruption events.

Our observations of Holuhraun plume in an early “young plume” state provide a valuable in-situ dataset for initialization of atmospheric models of the downwind plume dispersion to assess air quality and climate impacts. Few such in-situ measurements exist but are essential because the theoretical mechanisms dealing with plume dynamic and chemical processes are typically better known than the detailed composition of the volcano plume both near the crater or far from the source, as well as the actual injection altitudes of emissions which can vary in time during an eruption with compositionally distinct plume at different altitudes. In future, we will also undertake comparison of the data to measurements made far from the Holuhraun source, as well as inter-compare the Holuhraun volcanic aerosol to that of other volcanoes measured using the LOAC either by ground-based and balloon-based sampling, as well as remote sensing methods.

Acknowledgments.

The LOAC team of the LPC2E/CNRS warmly thank all the persons from Icelandic Meteorological Office and the University of Reykjavik for their supports during this field campaign, especially Evgenia Ilyinskaya and the Cambridge scientist teams who have accepted our presence in their field campaign. Special many thanks to Haraldur Olafsson for his welcome on Iceland and his generosity. Thanks to Richard Yeo and Njáll Fannar Reynisson for their remarkable professionalism and for the ride.

We acknowledge the ECMWF Archive product and Metview platform for permit the calculus of the backward trajectories. We also acknowledge the Icelandic team that produced the HARMONIE outputs.

This work is supported by the LABEX VOLTAIRE (ANR-10-LABX-100-01) from University of Orléans.

EC and RGG were supported by the NERC Centre for Observation and Modelling of Earthquakes, Volcanoes, and Tectonics (COMET) and from NERC grants NE/1015592/1 and NE/J023310/1.

References:

Arnalds, O.: Dust sources and deposition of aeolian materials in Iceland. Icelandic Agricultural Sciences 23:3–21, 2010.

Bagnold, R. A.: The Physics of Blown Sand and Desert Dunes, Methuen, New York, 1941.

Baratoux, D., Mangold, N., Arnalds, O., Bardintzeff, J.M., Platevoet, B., Grégorie, M., Pinet, P.: Volcanic sands of Iceland – Diverse origins of aeolian sand deposits revealed at Dyngjusandur and Lambahraun. Earth Surf. Proc. Land. 36:1789-1808, 2011.

Barsotti, S., Neri, A., Scire, J. S.: The VOL-CALPUFF model for atmospheric ash dispersal: 1. Approach and physical formulation, J. Geophys. Res., 113, B03208, doi:10.1029/2006JB004623, 2008.

Brousseaun, P., Berre, L., Bouttier, F., Desroziers, G.: Background-error covariances for a convective-scale data-assimilation system: AROME–France 3D-Var. Q. J. R. Meteorol. Soc. 137: 409–422. DOI:10.1002/qj.750, 2011.

Carboni, E., Grainger, R., Walker, J., Dudhia, A., Siddans, R.: A new scheme for sulphur dioxide retrieval from IASI measurements: application to the Eyjafjallajökull eruption of April and May 2010, Atmos. Chem. Phys., 12, 11417–11434, 2012/doi:10.5194/acp-12-11417-2012, 2012.

Carboni, E., Grainger, R. G., Mather, T. A., Pyle, D. M., Thomas, G., Siddans, R., Smith, A., Dudhia, A., Koukouli, M. L., and Balis, D.: The vertical distribution of volcanic SO2 plumes measured by IASI, Atmos. Chem. Phys. Discuss., 15, 24643-24693, doi:10.5194/acpd-15-24643-2015, 2015.

Chuan, R. L., Palais, J., Rose, W. I., Kyle, P. R.: Fluxes, sizes, Morphology and compositions of particles in the Mt. Erebus volcanic plume, December 1983, Journal of Atmospheric Chemistry 4 (1986), 467-477, 1986.

Dagsson-Waldhauserova, P., Arnalds, O., Olafsson, H.: Long-term frequency and characteristics of dust storm events in Northeast Iceland (1949-2011). Atmospheric Environment 77, 117-127, 2013.

Dagsson-Waldhauserova, P., Arnalds, O., Olafsson, H.: Long-term variability of dust events in Iceland. Atmospheric Chemistry and Physics 14, 13411-13422. DOI:10.5194/acp-14-13411-2014, 2014.

Deshler, T., Hervig, M. E., Hofmann, D. J., Rosen, J. M., Liley, J. B.: Thirty years of in situ stratospheric aerosol size distribution measurements from Laramie, Wyoming (41N), using balloon-borne instruments,J. Geophys. Res., 108(D5), 4167, doi:10.1029/2002JD002514, 2003.

Galle, B., Johansson, M., Rivera, C., Zhang Y., Kihlman, M., Kern, C., Lehmann T., Platt, U., Arellano, S., and S. Hidalgo (2010), Network for Observation of Volcanic and Atmospheric Change (NOVAC)—A global network for volcanic gas monitoring: Network layout and instrument description, J. Geophys. Res., 115, D05304, doi:10.1029/2009JD011823

Gíslason, S.R., Stefánsdóttir, G., Pfeffer, M.A., Barsotti, S., Jóhannsson, Th., Galeczka, I., Bali, E., Sigmarsson, O., Stefánsson, A., Keller, N.S., Sigurdsson, Á., Bergsson, B., Galle, B., Jacobo, V.C., Arellano, S., Aiuppa, A., Jónasdóttir, E.B., Eiríksdóttir, E.S., Jakobsson, S., Guðfinnsson, G.H., alldórsson, S.A., Gunnarsson, H., Haddadi, B., Jónsdóttir, I., Thordarson, Th., Riishuus, M., ögnadóttir, Th., Dürig, T., Pedersen, G.B.M., Höskuldsson, Á., Gudmundsson, M.T.: Environmental pressure from the 2014–15 eruption of Bárðarbunga volcano, Iceland. Geochem. Persp. Let. 1, 84-93, 2015.

Hammer, E., Gysel, M., Roberts, G. C., Elias, T., Hofer, J., Hoyle, C. R., Bukowiecki, N., Dupont, J.-C., Burnet, F., Baltensperger, U., Weingartner, E.: Size-dependent particle activation properties in fog during the ParisFog 2012/13 field campaign, Atmos. Chem. Phys, 2014/05/15 6.81, 2014.

Ialongo, I., Hakkarainen, J., Kivi, R., Anttila, P., Krotkov, N.AN, Yang, K., Li, C., Tukiainen, S., Hassinen, S., Tamminen, J.: Comparison of operational satellite SO2 products with ground-based observations in northern Finland during the Icelandic Holuhraun fissure eruption, Atmos. Meas. Tech. 2015, Vol. 8 Issue 6, p2279-2289. 11p. DOI:10.5194/amt-8-2279-2015, 2015.

Junge, C.E., Chagnon, C.W., Manson, J.E.: STRATOSPHERIC AEROSOLS. J. Meteor., 18, 81–108. doi: http://dx.doi.org/10.1175/1520-0469(1961)018<0081:SA>2.0.CO;2, 1961.

Kroll, J.H., Cross, E.S., Hunter, J.F, Pai, S., Wallace, L.M.M., Croteau, P.L., Jayne, J.T., Worsnop. D.R., Heald, C.L., Murphy, J.G., Frankel, S.L.: Atmospheric Evolution of Sulfur Emissions from Kīlauea: Real-Time Measurements of Oxidation, Dilution, and Neutralization within a Volcanic Plume. Environmental science & technology 49, no. 7: 4129-4137, 2015.

Martucci, G., Ovadnevaite, J., Ceburnis, D., Berresheim, S., Varghese, S., Martin, D., Flanagan, R., O'Dowd, C.D.: Impact of volcanic ash plume aerosol on cloud microphysics, Atmos. Env. 48 205-218, 2012.

McGonigle, A. J. S., Aiuppa, A., Giudice, G., Tamburello, G., Hodson, A. J., and Gurrieri, S.: Unmanned aerial vehicle measurements of volcanic carbon dioxide fluxes, Geophys. Res. Lett., 35, L06303, doi:10.1029/2007GL032508; 2008.

Oladottir, B., Larsen, G., Sigmarsson, O. : Holocene volcanic activity at Grímsvötn, Bárðarbunga and Kverkfjöll subglacial centres beneath Vatnajökull, Iceland. Bulletin of Volcanology 73,1187-1208, 2011.

Óladóttir, B.A., Sigmarsson, O., Larsen, G., Devidal, J.L. : Provenance of basaltic tephra from Vatnajökull subglacial volcanoes, Iceland, as determined by major- and trace-element analyses. The Holocene 21:1037–1048, 2011.

Oppenheimer C., Scaillet B., and Martin R. S.: Sulfur degassing from volcanoes: source conditions, surveillance, plume chemistry and earth system impacts." Reviews in mineralogy and geochemistry 73, no. 1, 363-421, 2011.

Pieri, D., Diaz, J.A., Bland, G., Fladeland, M., Madrigal, Y., Corrales, E., Alegria, O., et al. : In situ observations and sampling of volcanic emissions with NASA and UCR unmanned aircraft, including a case study at Turrialba Volcano, Costa Rica." Geological Society, London, Special Publications 380, no. 1: 321-352, 2013.

Renard, J.B., Berthet, G., Salazar, V., Catoire, V., Tagger, M., Gaubicher, B., Robert, C.: In situ detection of aerosol layers in the middle stratosphere, Geophys. Res. Lett., 37, L20803, doi:10.1029/2010GL044307, 2010.

Renard, J.B., Dulac, F., Berthet, G., Lurton, T., Vignelles, D., Jégou, F., Tonnelier, T., Thaury, C., Jeannot, M., Couté, B., Akiki, R., Verdier, N., Mallet, M., Gensdarmes, F., Charpentier, P., Duverger, V., Dupont, J.V., Mesmin, S., Elias, T., Crenn, V., Sciare, J., Giacomoni, J., Gobbi, M., Hamonou, E., Olafsson, H., Dagsson-Waldhauserova, P., Camy-Peyret, C., Mazel, C., Décamps, T., Piringer, M., Surcin, J., and Daugeron, D.: LOAC: a small aerosol optical counter/sizer for ground-based and balloon measurements of the size distribution and nature of atmospheric particles – Part 1:

Principle of measurements and instrument evaluation, Atmos. Meas. Tech. Discuss., 8, 9993-10056, doi:10.5194/amtd-8-9993-2015, 2015.

Rodgers, C.D.: Inverse Methods for Atmospheric Sounding: Theory and Practice, World Scientific Publishing Co. Ltd., 2000.

Roberts, T.J., Martin, R.S., Jourdain L.: Reactive bromine chemistry in Mount Etna's volcanic plume: the influence of total Br, high-temperature processing, aerosol loading and plume–air mixing, Atmospheric Chemistry and Physics, 14, 20, 11201-11219, 2014.

Roberts T.J., Vignelles D., Liuzzo M., Giudice G., Aiuppa A., Chartier M., Coute B., Lurton T., Berthet G., Renard J.-B.: Advances in in-situ real-time monitoring of volcanic emissions: HCl, and size-resolved aerosol at Mt Etna (passive degassing), submitted to Geochimica et Cosmochimica Act, 2015.

Saunders, R. W., Matricardi, M., and Brunel, P.: An improved fast radiative transfer model for assimilation of satellite radiance observations, Q. J. Roy. Meteor. Soc., 125, 1407–1425, doi:10.1002/qj.1999.49712555615 , 1999.

Shinohara, H.: Composition of volcanic gases emitted during repeating Vulcanian eruption stage of Shinmoedake, Kirishima volcano, Japan. Earth, Planets and Space, 65, 6: 667-675, 2013.

Schmidt, A., Leadbetter, S., Theys, N., Carboni,E., Withman, C.S., Stevenson, J.A., Birch, C.E., Thordarson, T., Turnock, S., Barsotti, S., Delaney, L., Feng, W., Grainger, R.G., Hort, M.C., Höskuldsson, À., Ialongo, I., Ilyinskaya, E., Jòhannsson, T., Kenny, P., Mather, T.A., Richards, N.A.D., Sheperd, J.: Satellite detection, long-range transport, and air quality impacts of volcanic sulfur dioxide from the 2014–2015 flood lava eruption at Bárðarbunga (Iceland), J. Geophys. Res. Atmos., 120, doi:10.1002/ 2015JD02363, 2015.

Schmidt, A., Ostro, B., Carslaw, K.S., Wilson, M., Thordarson, Th., Mann, G.W., Simmons A.J.: Excess Mortality in Europe Following a Future Laki-Style Icelandic Eruption. Proceedings of the National Academy of Sciences 108, no. 38: 15710–15. doi:10.1073/pnas.1108569108, 2011.

Spinetti, C., Barsotti, S., Neri, A., Buongiorno, M.F., Doumaz, F., Nannipieri, L.: Investigation of the complex dynamics and structure of the 2010 Eyjafjallajo¨ kull volcanic ash cloud using multispectral images and numerical simulations, J. Geophys. Res. Atmos., 118, 4729–4747, doi:10.1002/jgrd.50328, 2013.

Y. Seity, Brousseau, P., Malardel, S., Hello, G., Bénard, P., Bouttier, F., Lac, C., Masson, V.: The AROME-France Convective-Scale Operational Model. Mon. Wea. Rev., 139, 976–991, 2011.Spiridonov, V. and Curic, M.: Evaluation of the physical and chemical properties of Eyjafjallajökull volcanic plume using a cloud-resolving model. Pure and applied Geophysics. 170 (2013) 1729-1750, 2013.

Thordarson, T., and Self, S.: Atmospheric and Environmental Effects of the 1783–1784 Laki Eruption: A Review and Reassessment. J. Geophys. Res. 108, no. D1 (January 8, 2003): 4011., 2003.

Van Eaton, A. R., Herzog, M., Wilson, C.J.N., McGregor, J.: Ascent dynamics of large phreatomagmatic eruption clouds: The role of microphysics, J. Geophys. Res., 117, B03203, doi:10.1029/2011JB008892, 2012.

Vernier, J.-P., et al., Major influence of tropical volcanic eruptions on the stratospheric aerosol layer during the last decade, Geophys. Res. Lett., 38, L12807, doi:10.1029/2011GL047563, 2011.

Warner, J.: The Microstructure of Cumulus Cloud. Part I. General Features of the Droplet Spectrum. J. Atmos. Sci., 26, 1049–1059. doi: http://dx.doi.org/10.1175/1520-0469(1969)026<1049:TMOCCP>2.0.CO;2, 1969.

Warner, J.: The Microstructure of Cumulus Cloud. Part II. The Effect on Droplet Size Distribution of the Cloud Nucleus Spectrum and Updraft Velocity. J. Atmos. Sci., 26, 1272–1282. doi: http://dx.doi.org/10.1175/1520-0469(1969)026<1272:TMOCCP>2.0.CO;2, 1969.

Witham, C. S., Oppenheimer, C.: Mortality in England during the 1783–4 Laki Craters Eruption. Bulletin of Volcanology 67, no. 1 (May 11, 2004): 15–26. doi:10.1007/s00445-004-0357-7, 2004.

$$V(d) = \frac{V_0}{\sigma_N \sqrt{2\pi}} e^{\left(-\frac{1}{2}\left(\frac{\log(d)-\mu_v}{\sigma_N}\right)^2\right)} \quad (1)$$

Where $V(d)$ is the volume density distribution with shape parameters: σ_N and μ_v and the amplitude parameter V_0.

Equation 1. Calculated density distribution for the volume from shape parameters giving by less-square fitting

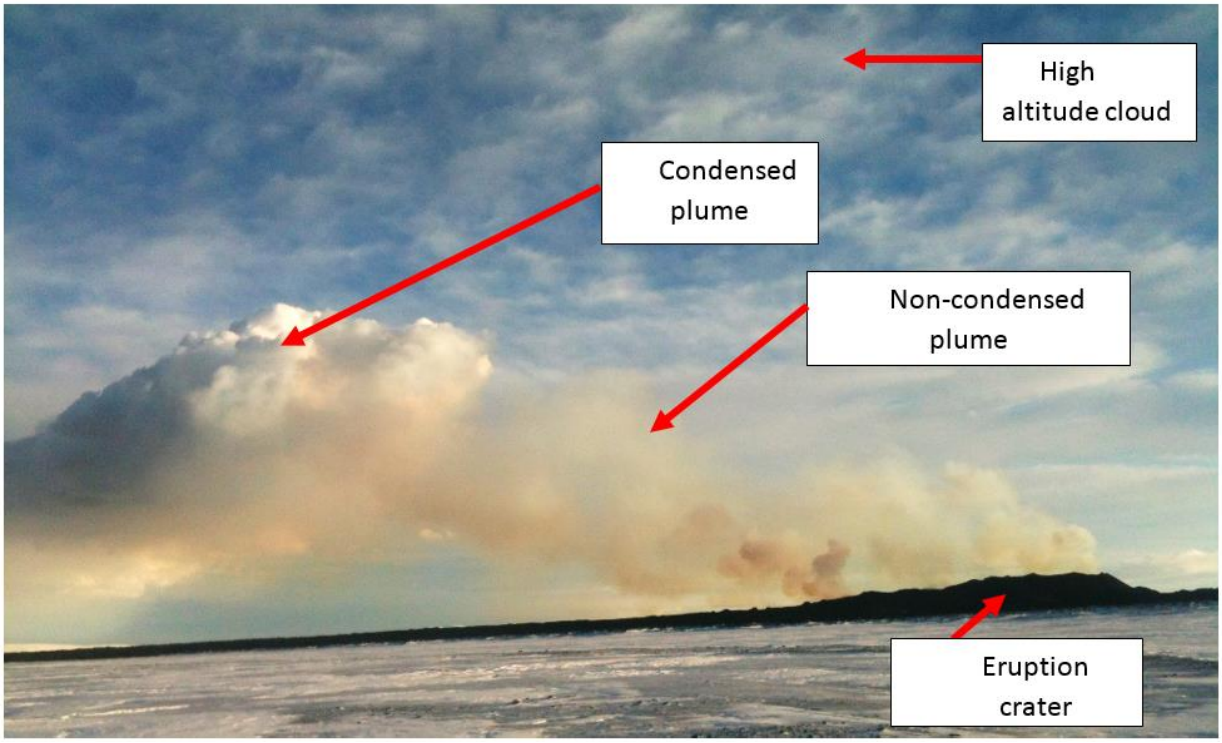

Figure 1. Picture taken at 14UTC on January 22nd during the afternoon before the balloon flight.

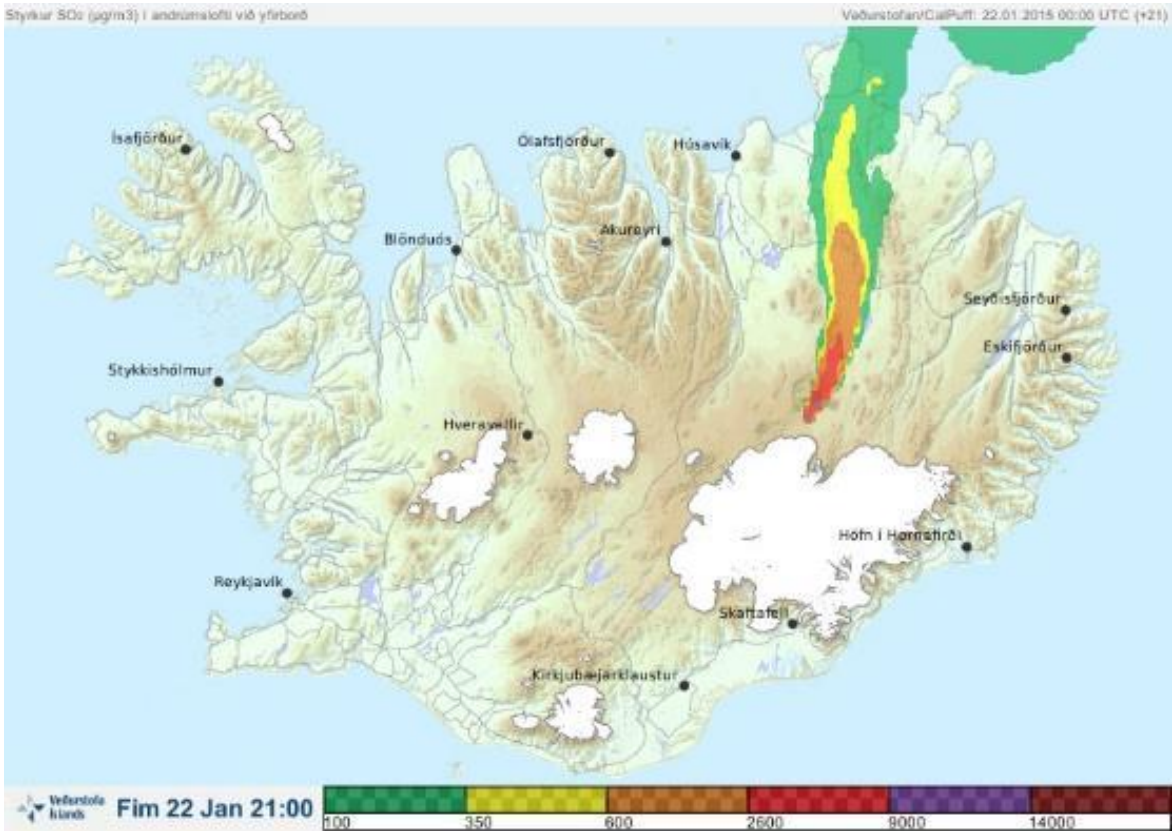

588
589 **Figure 2.** Forecast from the Icelandic Meteorological Office showing the direction of the plume
590 and the concentration in µg/m^3 of SO2 at 22UTC on the January 22th, less than 30 minutes before
591 the balloon launch. This forecast was used on the campaign field in order to take the decision to
592 launch the balloon. During the daytime the plume direction was going to the East, which didn't
593 represented a good solution for make the balloon borne profile near to the crater.
594

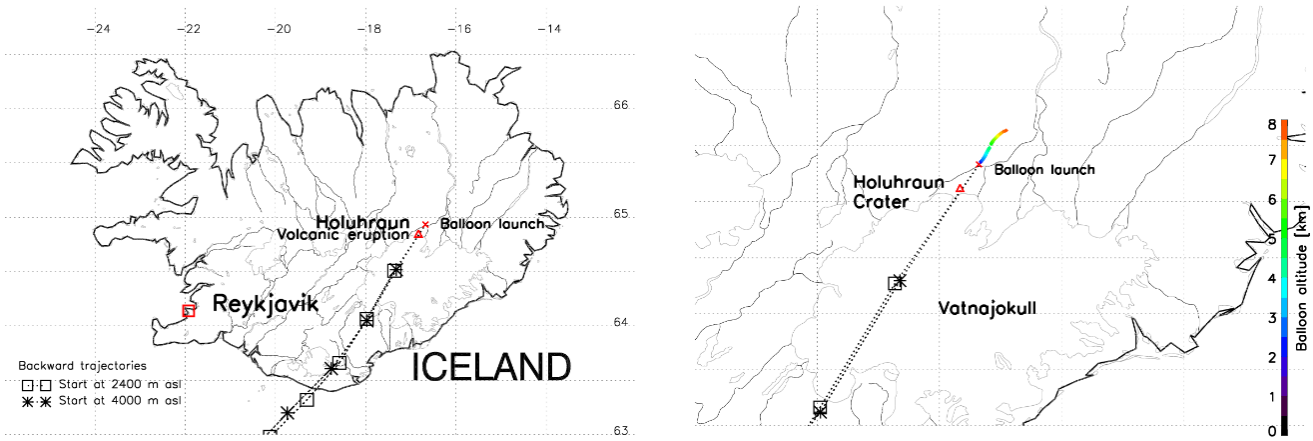

Figure 3. Localization of the launch, on the left: general view, the Holuhraun eruption is located by a red triangle and the balloon launch by a red cross. On the right: focus on the Holuhraun crater, the balloon flight path is represented as a function of altitude referred by the key on the right. For both panels, we add two time backward trajectories intersecting the balloon launch position at 2400 m and 4000m. These trajectories are calculated using FLEXTRA code initialized with ECMWF wind fields of January 22nd at 21UTC above the balloon launch position.

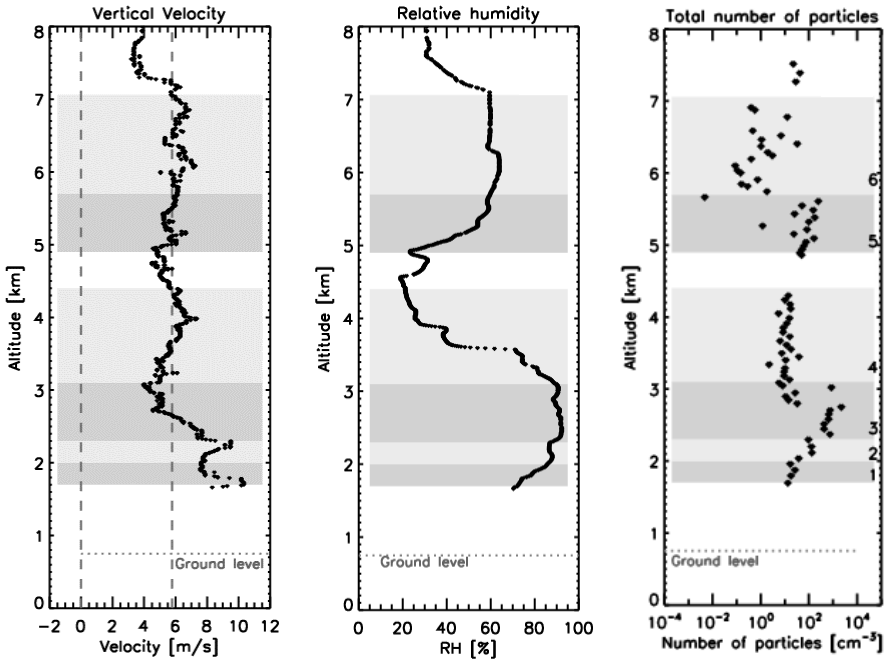

602 **Figure 4.** Flight parameters measured during the balloon ascent. A: Vertical velocity, B: Relative
603 humidity, C: Total particles concentration (from 0.2 to 100µm).

604

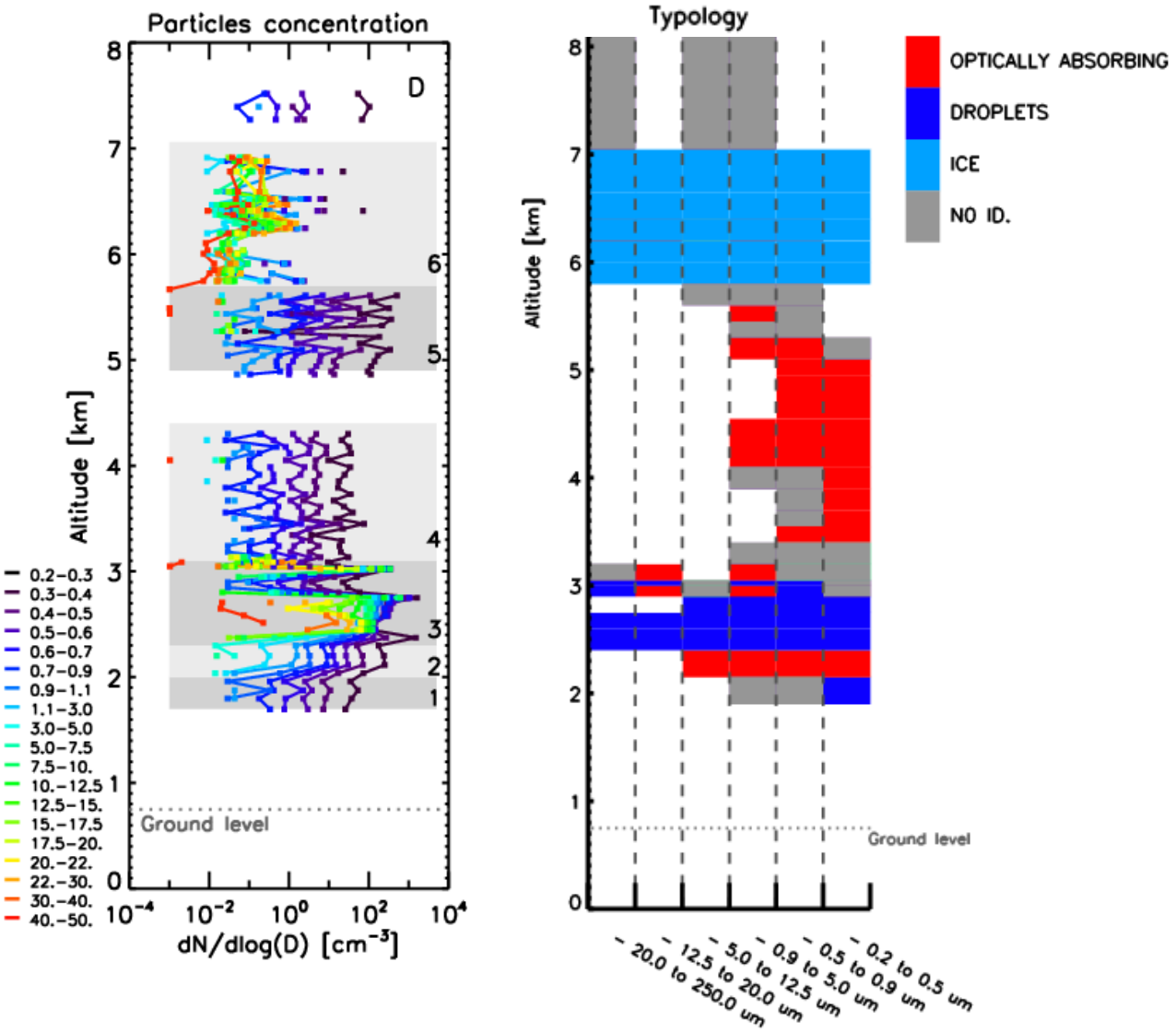

605 **Figure 5.** On the left: Normalized concentration of aerosols for each size class as a function of
606 altitude. Each color is relative to a size class, the key is on the left. On the right and for the same
607 altitudes, Typology : main optical nature for 6 super-size classes as a function of altitude.
608

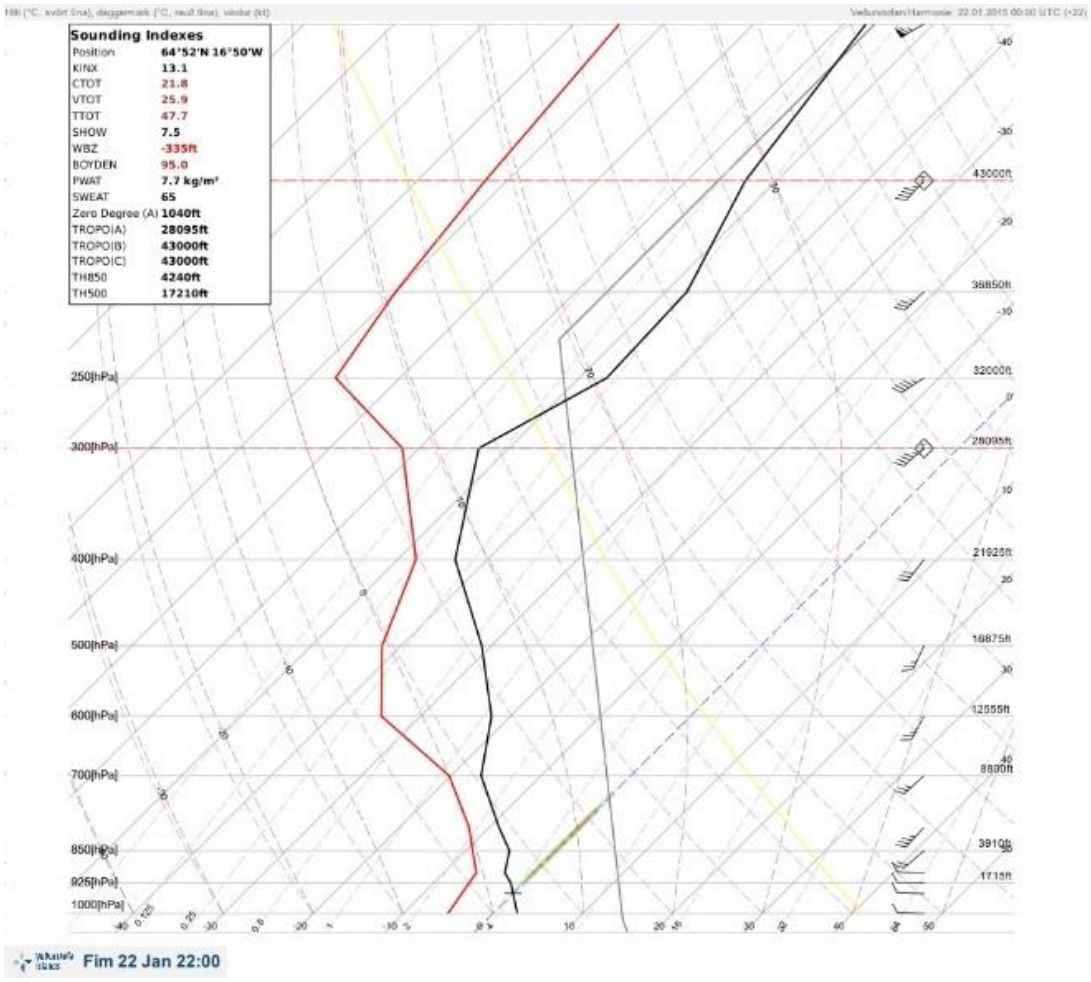

Figure 6. Outputs from the HARMONIE model for the Holuhraun region (64°52'N and 16°50'W) over a 2.5 km square region, showing the column profile over the fissural eruption at 22UTC, time of the balloon launch. The red line represents the dew point and the black line the temperature simulated. When the temperature and the dew point match the air is saturated and we expect a cloud. Here, the model does not predict any cloud.

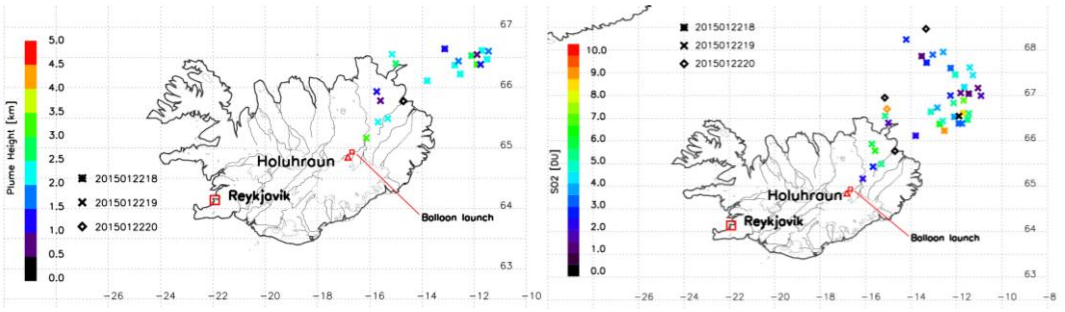

Figure 7. Left: height of the plume for three overpasses at 18, 19 and 20UTC on January 22th from IASI retrieval method in Carboni et al. 2012. Right: SO2 in Dobson units for the same three overpasses.

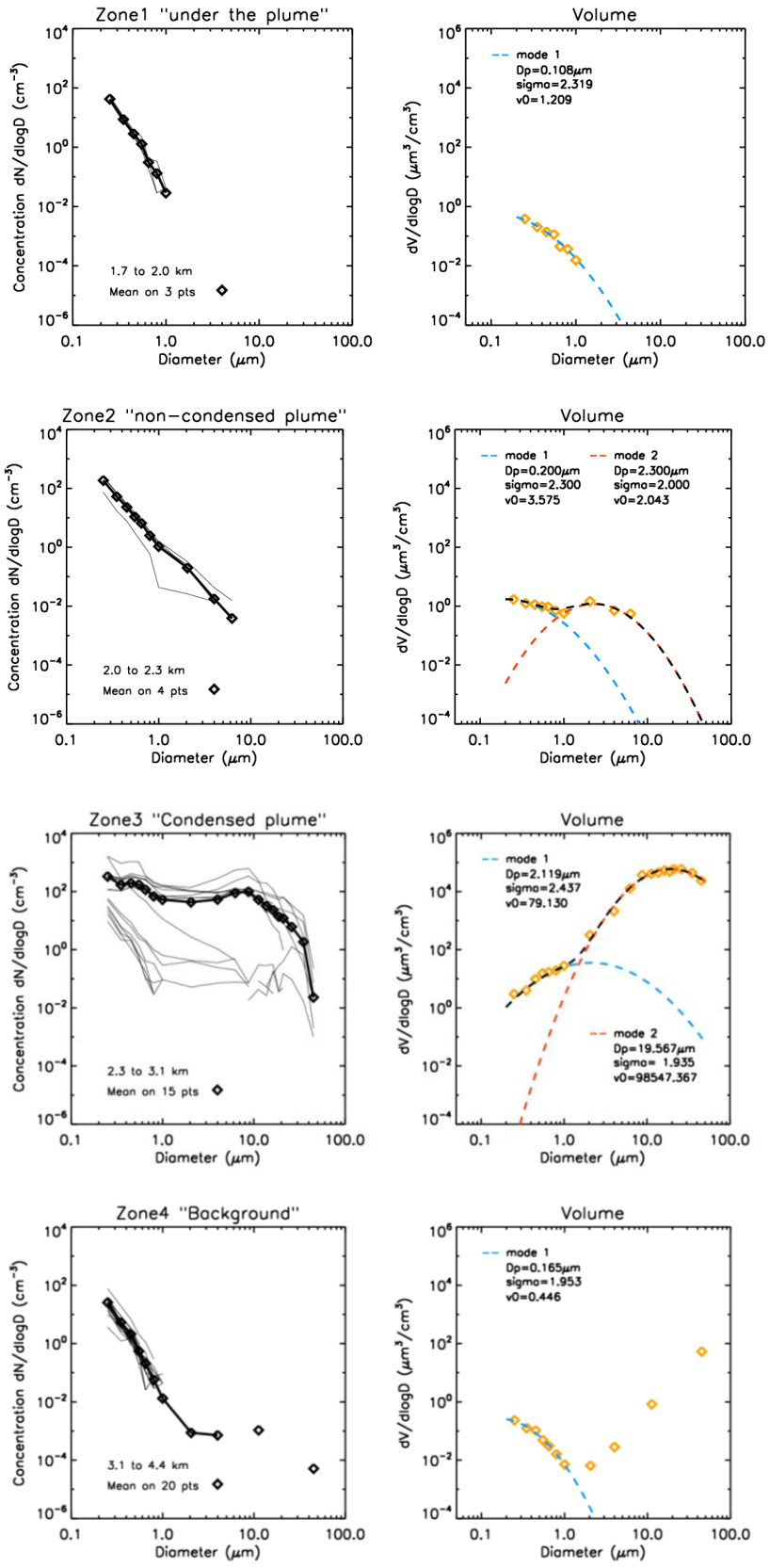

Figure 8: Size-distribution by number and by volume with lognormal fit for the zone 1 to 4.

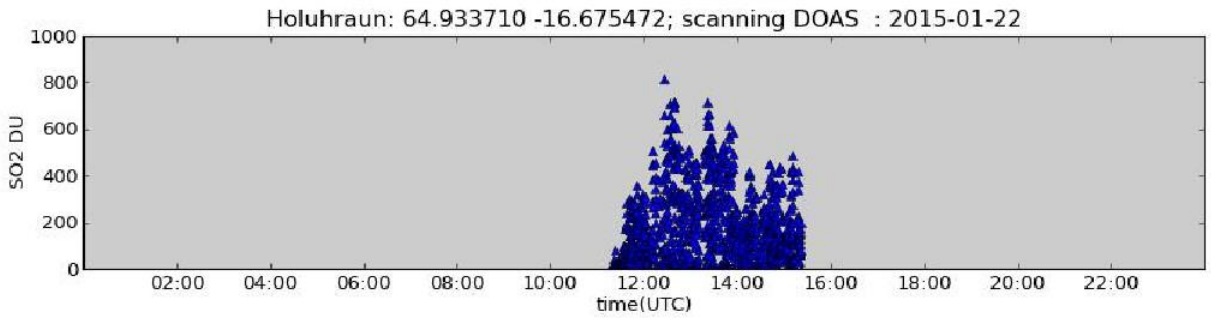

Figure 9. Time series on January 22nd 2015 of the column density of SO2 detected by NOVAC scanning DOAS positioned 10 km from the eruption site. An average emission rate of 400 kg/s SO2 for this day is calculated.

	Zone 1	Zone 2		Zone 3		Zone 4
	From 1.7 to 2.0 km	From 2.0 to 2.3 km		From 2.3 to 3.1 km		From 3.1 to 4.4 km
	Under the plume	*Non-condensed plume*		*Condensed plume*		*Background*
		Mode 1	Mode 2	Mode 1	Mode 2	
Mean diameter [µm]	0.1	0.2	2.3	2.1	19.6	0.1
Standard deviation [µm]	2.3	2.3	2.0	2.4	1.9	2.0
Total volume [μm^3]	1.2	3.6	2.0	79.1	98547.3	0.4

633

634 Table 1: Parameters from the log-normal fitting on volumic concentration measured by LOAC for
635 the first four zones determined. Zone 1 and zone 4 are assumed as the “clean” air mass in which the
636 plume is advected and measured in zone 2 and 3.

637